

| | |
|--------------------------------|---|
| Titre: Title: | Numerical simulations with the P-Hydroslag model to predict phosphorus removal by steel slag filters |
| Auteurs: Authors: | Dominique Claveau-Mallet, Benoit Courcelles, Philippe Pasquier et Yves Comeau |
| Date: | 2018 |
| Type: | Article de revue / Journal article |
| Référence: Citation: | Claveau-Mallet, D., Courcelles, B., Pasquier, P. & Comeau, Y. (2017). Numerical simulations with the P-Hydroslag model to predict phosphorus removal by steel slag filters. <i>Water Research</i> , 126, p. 421-432. doi: 10.1016/j.watres.2017.09.032 |



Document en libre accès dans PolyPublie

Open Access document in PolyPublie

| | |
|---|---|
| URL de PolyPublie: PolyPublie URL: | https://publications.polymtl.ca/3134/ |
| Version: | Version finale avant publication / Accepted version Révisé par les pairs / Refereed |
| Conditions d'utilisation: Terms of Use: | CC BY-NC-ND |



Document publié chez l'éditeur officiel

Document issued by the official publisher

| | |
|---|---|
| Titre de la revue: Journal Title: | Water Research (vol. 126) |
| Maison d'édition: Publisher: | Elsevier |
| URL officiel: Official URL: | https://doi.org/10.1016/j.watres.2017.09.032 |
| Mention légale: Legal notice: | "In all cases accepted manuscripts should link to the formal publication via its DOI" |

**Ce fichier a été téléchargé à partir de PolyPublie,
le dépôt institutionnel de Polytechnique Montréal**

This file has been downloaded from PolyPublie, the
institutional repository of Polytechnique Montréal

<http://publications.polymtl.ca>

1 Numerical simulations with the P-Hydroslag model to predict phosphorus removal
2 by steel slag filters

3 By Dominique Claveau-Mallet*, Benoît Courcelles, Philippe Pasquier, and Yves Comeau

4 Department of Civil, Geological and Mining Engineering, Polytechnique Montreal, Montreal, Quebec,
5 Canada, H3C 3A7

6 * corresponding author: Dominique.claveau-mallet@polymtl.ca

7 ABSTRACT

8 The first version of the P-Hydroslag model for numerical simulations of steel slag filters is presented.
9 This model main original feature is the implementation of slag exhaustion behavior, crystal growth and
10 crystal size effect on crystal solubility, and crystal accumulation effect on slag dissolution. The model
11 includes four mineral phases: calcite, monetite, homogeneous hydroxyapatite (constant size and
12 solubility) and heterogeneous hydroxyapatite (increasing size and decreasing solubility). In the proposed
13 model, slag behavior is represented by CaO dissolution kinetic rate and exhaustion equations; while slag
14 dissolution is limited by a diffusion rate through a crystal layer. An experimental test for measurement
15 of exhaustion equations is provided. The model was calibrated and validated with an experimental
16 program made of three phases. Firstly, batch tests with 300g slag sample in synthetic solutions were
17 conducted for the determination of exhaustion equation. Secondly, a slag filter column test fed with
18 synthetic solution was run for 623 days, divided into 9 cells and sampled at the end of the experiment.
19 Finally, the column was dismantled, sampled and analyzed with XRD, TEM and SEM. Experimental
20 column curves for pH, oPO_4 , Ca and inorganic carbon were well predicted by the model. Crystal sizes
21 measured by XRD and TEM validated the hypothesis for homogeneous precipitation while SEM
22 observations validated the thin crystal layer hypothesis.

23 KEYWORDS

24 slag, phosphorus, wastewater treatment modelling, PHREEQC, hydroxyapatite, calcite, precipitation

25 ABBREVIATIONS

| 26 | Symbol | Description |
|----|-------------------------------------|-----------------------------------|
| 27 | <u>General abbreviations</u> | |
| 28 | BOF | Basic oxygen furnace |
| 29 | CW | Constructed wetlands |
| 30 | EAF | Electric arc furnace |
| 31 | HRT _v | Hydraulic retention time of voids |
| 32 | MONtoHAP | Transformation of MON into HAP |
| 33 | o-PO ₄ | Ortho-phosphates |
| 34 | SEM | Scanning electron microscope |
| 35 | TEM | Transmission electron microscope |
| 36 | TIC | Total inorganic carbon |
| 37 | WW | Wastewater |
| 38 | XRD | X-Ray diffraction |

39 **Abbreviations for mineral phases**

| | | | |
|----|--------|--|---|
| 40 | CAL | Calcite | CaCO ₃ |
| 41 | HAP | Hydroxyapatite | Ca ₅ OH(PO ₄) ₃ |
| 42 | HAP_HO | Primary hydroxyapatite via homogeneous precipitation | Ca ₅ OH(PO ₄) ₃ |
| 43 | HAP_HE | Primary hydroxyapatite via heterogeneous precipitation | Ca ₅ OH(PO ₄) ₃ |
| 44 | HAP2 | Secondary hydroxyapatite via monetite transformation | Ca ₄ OH ₂ (PO ₄) ₂ |
| 45 | MON | Monetite | CaHPO ₄ |

46 **Symbol** **Description** **Units (value)**

47 **Constants**

| | | | |
|----|-----------------|---|---------------------------------|
| 48 | a_{HAP_0} | HAP crystal size in homogeneous precipitation | [m] |
| 49 | B_1 and B_2 | Regression coefficients in k_{diss} exhaustion function | |
| 50 | D^* | Dispersivity (transport model) | [cm] |
| 51 | D_n | Exchange factor between effective and immobile porosity (transport model) | [s ⁻¹] |
| 52 | k_{CAL} | CAL precipitation constant | [mol CAL/s m ² slag] |
| 53 | k_{HAP} | HAP precipitation constant | [mol HAP/s m ² slag] |
| 54 | k_{MON} | MON precipitation constant | [mol MON/s m ² slag] |
| 55 | $k_{MONtoHAP}$ | MONtoHAP precipitation constant | [M HAP2/(M MON s)] |
| 56 | K_{spCAL} | Solubility product for CAL | [M ²] |

| | | | |
|----|--|--|---|
| 57 | K_{spHAP_bulk} | Bulk solubility product for HAP | [10 ⁻⁵⁷ M ⁹] |
| 58 | K_{spHAP_HO} | Solubility product for HAP_HO | [M ⁹] |
| 59 | K_{spMON} | Solubility product for MON | [M ²] |
| 60 | L_{HAP} | L/D ratio for columnar HAP crystals | [-] |
| 61 | mv_{exp} | Slag mass to water volume ratio in a batch test | [g/mL] |
| 62 | MW_{HAP} | HAP Molecular weight | [502 g/mol] |
| 63 | n | Total porosity in the slag filter | [-] |
| 64 | n_e | Effective porosity in the slag filter | [-] |
| 65 | n_{im} | Immobile porosity in the slag filter | [-] |
| 66 | P_1, P_2, P_3 and P_4 | Regression coefficients in pH_{sat} exhaustion function | |
| 67 | R | Ideal gas constant | [8.31 J mol ⁻¹ K ⁻¹] |
| 68 | S | Slag specific surface | [m ² /m ³] |
| 69 | se_{HAP_0} | initial HAP seeds concentration | [seeds/L] |
| 70 | SI_c | Critical saturation index between HAP_HE and HAP_HO | [-] |
| 71 | T | Temperature | [K] |
| 72 | γ | HAP mean free surface energy | [87 mJ/m ³] |
| 73 | ρ_{barr} | Crystal concentration in the crystal barrier | [g crystal/m ³] |
| 74 | ρ_{HAP} | HAP crystal density | [3 600 000 g/m ³] |
| 75 | ρ_{slag} | Slag grain density | [3.8 g/mL] |
| 76 | <u>Rates, functions and variables</u> | | |
| 77 | a_{HAP} | Mean HAP crystal size | [m] |
| 78 | b_{im} | Moles of an element in immobile porosity (transport model) | [mol] |
| 79 | C | Total dissolved concentration for an element (transport model) | [mol/kgw] |
| 80 | C_e | C in effective porosity (transport model) | [mol/kgw] |
| 81 | C_{im} | C in immobile porosity (transport model) | [mol/kgw] |
| 82 | $CaOl_{BATH}$ | Leached CaO in a acid bath | [mol/g] |
| 83 | CaO_{KTEST} | Leached CaO in a batch test | [mol/g] |
| 84 | $CaOl_{TOT}$ | Cumulative leached CaO in a batch test | [mol/g] |
| 85 | D_{barr} | Diffusion coefficient in the crystal barrier | [m ² /s] |
| 86 | d_{barr} | Thickness of the crystal barrier | [m] |
| 87 | k_{diss} | Slag dissolution constant | [mol CaO/m ² slag] |

| | | | |
|-----|-----------------|---|-------------------------|
| 88 | K_{spHAP_HE} | Solubility product for HAP_HE | [M ⁹] |
| 89 | pH_{sat} | Saturation pH in the slag filter | [-] |
| 90 | q | Concentration in the solid phase for an element (transport model) | [mol/kgw] |
| 91 | r_{CAL} | CAL precipitation rate | [M CAL/s] |
| 92 | r_{diff} | CaO diffusion rate through crystal barrier | [M CaO/s] |
| 93 | r_{diss} | Slag dissolution rate | [M CaO/s] |
| 94 | r_{HAP_HE} | Primary heterogeneous HAP precipitation rate | [M HAP/s] |
| 95 | r_{HAP_HO} | Primary homogenous HAP precipitation rate | [M HAP/s] |
| 96 | r_{MON} | MON precipitation rate | [M MON/s] |
| 97 | $r_{MONtoHAP}$ | Secondary HAP precipitation rate | [M HAP ² /s] |
| 98 | S_{HAP} | HAP molar specific surface | [m ² /mol] |
| 99 | se_{HAP} | HAP seeds concentration | [units/L] |
| 100 | SF_{diff} | Step function in diffusion rate | [-] |
| 101 | SF_{diss} | Step function in dissolution rate | [-] |
| 102 | SF_{HAP_HE} | Step function in HAP_HE rate | [-] |
| 103 | SF_{HAP_HO} | Step function in HAP_HO rate | [-] |
| 104 | SI_{HAP_HE} | Saturation index for HAP_HE | [-] |
| 105 | SI_{HAP_HO} | Saturation index for HAP_HO | [-] |
| 106 | t | Time (transport model) | [s] |
| 107 | v | Pore water flow velocity (transport model) | [m/s] |
| 108 | x | 1D distance (transport model) | [m] |
| 109 | X_{CaO} | Total leached CaO in the slag filter | [M] |

110

111 1 Introduction

112 Steel slag filters are an effective and passive technology for phosphorus removal from wastewater,
113 allowing typical municipal effluent o-PO₄ concentration below 0.5 mg P/L (Koiv et al., 2016). Design tools
114 for slag filters are not yet developed and full scale slag filters cannot be implemented without expensive
115 pilot tests. The main issue related to steel slag filter operation relies on filter exhaustion and a relatively
116 rapid drop of removal efficiency (Chazarenc et al., 2008). A tool providing the effect of influent

117 composition and operational conditions (type and size of slag, influent flowrate, filter geometry) on slag
118 filter effluent o-PO₄ concentration and longevity would facilitate the design of these systems. This paper
119 presents the P-Hydroslag model, a new model adapted for steel slag filter simulations considering
120 influent composition and void hydraulic retention time (HRT_v) while being compatible with accepted
121 physicochemical modeling frameworks (Lizarralde et al., 2015; Mbamba, Batstone et al., 2015; Mbamba,
122 Tait et al., 2015).

123 Sorption isotherms were largely proposed as a design tool for steel slag filters (Vohla et al., 2011), but
124 this method does not consider void precipitation and long-term changes in the material properties,
125 explaining why isotherms could not yet predict correctly full-scale behavior. The k-C* model traditionally
126 used for constructed wetlands (Kadlec and Wallace, 2009) successfully predicted steel slag filter
127 performance (Barca et al., 2013). This method may be suitable for design, but it cannot estimate the
128 lifetime of the filter. A general correlation between material CaO content and P retention capacity based
129 on several studies was proposed by Vohla et al. (2011), highlighting the importance of CaO dissolution in
130 retention mechanisms. Such a design tool, however, does not consider important aspects as CaO
131 availability, HRT_v or influent composition, leading to a prediction uncertainty that is not acceptable for
132 design purpose. Finally, a predictive model based on several material properties, HRT_v and inlet P
133 concentration was proposed (Penn et al., 2016). This model's strengths were to consider both Fe-Al and
134 Ca based materials, propose an empiric relationship between material buffering capacity and P
135 retention capacity, and predict P retention for both lab-scale and pilot-scale systems. This model,
136 however, did not include direct measurement of kinetic rates, and would not be compatible with
137 general physicochemical modeling frameworks in wastewater treatment.

138 Two previous modeling studies were published in the recent years. The first study (Claveau-Mallet et al.,
139 2012) qualitatively described concepts forming the basis of the model, including slag dissolution,
140 hydroxyapatite precipitation, crystal formation and accumulation in voids, and effect of velocity on

141 crystal accumulation. In the second study (Claveau-Mallet et al., 2014), concepts were translated into a
142 prototype model including mathematical equations for precipitation and slag exhaustion, and a
143 proposition of laboratory protocol for slag characterization was presented. Numerical simulations of a
144 slag filter were performed on the base of this prototype model without experimental program for
145 calibration. Results were realistic but overestimated the filter longevity. Predictions from the 2014
146 prototype model were compared to full-scale real data in a recent study (Koiv et al., 2016) in which
147 longevity was overestimated.

148 In this paper, the first full version of the P-Hydroslag (standing for Phosphorus-hydroxyapatite-slag)
149 model is presented. The P-Hydroslag model is similar to the 2014 prototype model, with additional
150 features for diffusion barrier and crystal growth, a refined characterization of exhaustion equations, and
151 a complete model equation matrix. The objectives were to calibrate the P-Hydroslag model with
152 experimental data and evaluate the validity and realism of the model.

153 2 Material and Methods

154 2.1 Slag media

155 5-10 mm electric arc furnace steel slag produced by Arcelor Mittal and provided by Minéraux Harsco
156 (Contrecoeur, Canada) was used (33% Fe₂O₃, 30% CaO, 16% SiO₂, 12% MgO, 6% Al₂O₃ and 3% other
157 metallic oxides). Its density (3.8) and specific surface (0.308 m²/g) were determined according to the
158 ASTM C127-04 standard (ASTM, 2004) and the Brunauer, Emmet and Teller method (Lowell et al., 2004).
159 Slag from the same source was previously studied by the authors' research team for wastewater
160 treatment applications (Claveau-Mallet et al., 2015; Claveau-Mallet et al., 2013; Koiv et al., 2016) or
161 modeling studies (Claveau-Mallet et al., 2014; Claveau-Mallet et al., 2012).

162 2.2 Column test

163 A vertical filter column filled with slag was fed from its base with a synthetic wastewater in a saturated
164 mode for a total duration of 623 days at approximately 25°C. The column size was 159 cm in length
165 and 10 cm in internal diameter. The synthetic wastewater solution consisted of K_2HPO_4 , KH_2PO_4 , $NaHCO_3$
166 and $CaCl_2$ in tap water. The influent mean composition was pH of 7.80 ± 0.2 , ortho-phosphates (o- PO_4)
167 of 8.9 ± 2.0 mg P/L, total inorganic carbon (TIC) of 22 ± 2 mg C/L, Ca of 54 ± 14 mg/L and alkalinity of 102
168 ± 3 mg $CaCO_3$ /L. The influent flowrate was 6.9 ± 1.0 mL/min for the first 517 days and 3.4 ± 0.5 mL/min
169 for the remaining 106 days of operation.

170 The column was divided into 11 virtual cells for the filling step, identified #0 to #10, with #0 at bottom
171 (inlet) and #10 at top (outlet). Cells #1 to #9 were 15 cm long and had a sampling hole in the middle.
172 Cells #0 and #10 were 7.5 cm long and had no sampling hole to provide a slag transition zone between
173 the inlet/outlet tubing and sampling zones. While filling the column, two 300 g slag samples were taken
174 from each cell using a standard sampling procedure for aggregate materials (ASTM C702, 2011). Slag
175 samples were used in batch kinetic tests (presented in section 2.3). The total slag mass in the column
176 was 24.24 kg, resulting in a 49.2% porosity.

177 The feeding barrel, column effluent and cells were sampled and analyzed periodically for pH, o- PO_4 ,
178 filtered Ca, settled TIC, total P and alkalinity, using standard procedures (APHA, AWWA and WEF, 2005).

179 A maximum of 3 cells were sampled in the same day to minimize perturbation, resulting in a monthly
180 sampling frequency for each cell (twice a month in the second feeding phase). The feeding barrel and
181 effluent column sampling frequency was weekly for pH and once or twice a month for the other
182 parameters. Tracer tests were conducted after 12, 69, 82, 107, 187, 271, 376 and 558 days. Rhodamine
183 at a concentration of 20 mg/L was used as a tracer and measured in the effluent using
184 spectrofluorometry.

185 At the end of operation, feeding was stopped and the column was kept saturated for 6 days before
186 dismantling. Upon dismantling, pore water was first sampled and analyzed, then the column was cut

187 into 4 sections to ensure efficient solids sampling. For each cell, three samples were taken: first, several
188 slag particles sampled before doing any major disturbance of the slag media (for scanning electron
189 microscope (SEM) analysis); then slag was washed with water in a large pan and precipitates were
190 sampled by sedimentation (for X-ray diffraction (XRD) and transmission electron microscope (TEM)
191 analyses); finally, a 300 g of washed slag sample was taken for kinetic tests (described in section 2.3).
192 Precipitates were air-dried for 3 days, sieved at mesh 60 and cleaned from slag dust with a strong
193 magnet. Precipitates were analyzed with XRD using a Philipps X'Pert diffractometer operated at 50 kV
194 and 40 mA, using the Bragg-Brentano geometry and a $\text{CuK}\alpha$ radiation. The Scherrer equation (Cullity,
195 2001) was used to estimate mean crystal sizes from diffractograms, using the $\sim 26.1^\circ$ peak for
196 hydroxyapatite (HAP) and $\sim 29.4^\circ$ peak for calcite (CAL). Precipitates of cells 1, 2, 3 and 8 were analyzed
197 using TEM with the bright field imaging technique (Jeol JEM-2100f field emission gun microscope, 200
198 kV). Before TEM analysis, samples were prepared with a 30-s ultrasound bath in methanol, and placed
199 on a copper grid covered with Formvar lightly coated with amorphous carbon. Undisturbed slag
200 particles of cells 1, 2, 3, 5 and 8 were analyzed with SEM using a Jeol JSM-7600F microscope (2.0 kV, LEI
201 or SEI detector).

202 2.3 Batch kinetic tests

203 The batch kinetic test method is described in another reference (Claveau-Mallet et al., 2014) and is
204 intended to produce exhaustion equations. The batch test included 5 identical phases. In a phase, the
205 slag sample was placed in a 1L Erlenmeyer flask containing 350 or 700 mL of a wastewater solution. The
206 Erlenmeyer flask was placed in a gyratory shaker at 160 rpm. The flask was closed with a rubber cap that
207 contained three airtight holes; one for a pH probe, one for a sampling tubing and one for a tubing
208 connected to a N_2 gas balloon. The synthetic solution was composed of KH_2PO_4 , K_2HPO_4 , NaHCO_3 and
209 CaCl_2 dissolved in tap or distilled water. Four solutions with different concentrations were used to test
210 the method in a realistic range of wastewater types (pH of 6.5 to 7.9, o- PO_4 of 8 to 24 m P/L, Ca of 17 to

211 50 mg/L, TIC of 0.5 to 24 mg C/L and alkalinity of 3 to 107 mg CaCO₃/L). At time zero, slag was inserted.
212 pH was monitored for 3 to 4 days. Three intermediary 20-mL samples were taken and analyzed for o-
213 PO₄, filtered Ca and filtered TIC. When necessary, a linear correction against time was applied to pH
214 measurements to account for probe drift. After this test, the slag sample was rinsed and immediately
215 transferred to a 160 rpm shaken HNO₃ acid bath of known volume and concentration for 3 to 5 days.
216 After the acid bath, pH was measured and the corresponding leached CaO from the slag was computed
217 using numerical simulations (explained in section 2.5.2). After the acid bath, the slag sample was
218 carefully rinsed and used again for a subsequent phase.

219 Each 300-g slag sample from cells 1 to 8 was used for a 5-phase kinetic test, resulting in 16 kinetic tests
220 (2 replicates per cell). One-phase batch tests on dismantled column slag samples were performed for
221 cells 1 to 9.

222 2.4 Model description

223 2.4.1 Precipitation

224 The model's Gujer matrix is presented in appendix. Three mineral phases are included: HAP typically
225 found in slag filters (Baker et al., 1998), monetite (MON) as intermediary phase and CAL. The
226 transformation of MON into HAP (MONtoHAP) was modelled as precipitation of HAP2, an artificial phase
227 composed of ions missing from MON before being HAP. Precipitation rates for HAP, MON and CAL were
228 formulated with a basic expression rate = $k \times SI$, with k being a constant normalized with slag surface and
229 SI the saturation index. The bulk solubility constant for HAP (K_{spHAP_bulk}) was set at 10^{-57} (Stumm and
230 Morgan, 1996a), within the 10^{-55} to 10^{-63} range reported in the literature (Lundager Madsen, 2008;
231 Oelkers et al., 2009; Parkhurst and Appelo, 1999; Stumm and Morgan, 1996a). K_{spCAL} was set at $10^{-7.5}$,
232 assuming an intermediary state between crystalline calcite ($10^{-8.48}$, PHREEQC database (Parkhurst and

233 Appelo, 1999)) and hydrated calcium carbonate ($10^{-7.144}$, MINTEQ database (Allison et al., 1991)).

234 K_{spMON} was set at 10^{-7} from Valsami-Jones (Valsami-Jones, 2001).

235 Two types of HAP were included to account for two types of precipitation. HAP_HO was HAP formed by

236 homogeneous precipitation (new seeds precipitated in voids, or spontaneous precipitation) while

237 HAP_HE was HAP formed by heterogeneous precipitation (on existing surfaces - crystal growth). HAP_HE

238 occurred below a critical saturation index (SI_c) while HAP_HO occurred over SI_c . In homogeneous

239 precipitation, crystal size was assumed to be constant. Using equation 1 for solubility of fine particles

240 (Stumm and Morgan, 1996b), K_{spHAP_HO} was set at 10^{-46} . Temperature was set at 298 K and specific

241 surface (S_{HAP}) was calculated assuming crystal size $a_{HAP_0} = 31.3$ nm, columnar shape for HAP and a

242 L/D ratio (L_{HAP}) of 50. The value assumed for a_{HAP_0} is close to crystal size measured in this study

243 (presented in a following section) and measurements made in previous studies (Claveau-Mallet et al.,

244 2012, 2013). A value of 10^{-46} for K_{spHAP_HO} is consistent with equilibrium state generally observed in

245 slag filters, assumed when effluent pH is over 10 with high HRT_v (Table 1 and Figure 1). In Table 1, Ca^{2+} ,

246 OH^- and PO_4^{3-} activities were determined with PHREEQC and used for apparent solubility calculation.

247 Studies conducted with hydrated oil shale ash were included in Table 1 as they behave in a similar way

248 then slag. Resulting mean and median were $10^{-45.7}$ and $10^{-46.0}$ from 389 data points.

$$249 \log(K_{spHAPHO}) = \log(K_{spHAPbulk}) + \frac{2}{3} \frac{\gamma S_{HAP}}{2.3RT} \quad [1]$$

250 **Table 1.** Apparent HAP solubility from reported alkaline filter effluent with pH \geq 10, based on reported

251 pH, Ca and o-PO₄ concentration.

| Material | Size (mm) | Influent | Type of study | Apparent log K _{sp} of HAP | | Re f | Nb of data points |
|----------|-----------|----------|---------------|-------------------------------------|--------|------|-------------------|
| | | | | mean | median | | |
| Sas | 5-10 | Solution | lab – column | -45.55 | -45.94 | 1 | 35 |

| | | | | | | | |
|--------------------------|-----------|------------------------|----------------|--------|--------|---|-----|
| EAF slag | 5-10 | Solution | lab – column | -45.18 | -45.72 | 2 | 103 |
| Sas | 2.5-5 | Solution | lab – column | -48.06 | -48.17 | 3 | 6 |
| Sas | 5-10 | real fishfarm WW | pilot – column | -45.23 | -45.39 | 4 | 46 |
| Hydr. Oil shale ash | 5-20 | real domestic WW | pilot – CW | -46.32 | -46.52 | 5 | 62 |
| Hydr. Oil shale ash | 5-20 | real landfill leachate | pilot – CW | -46.55 | -46.42 | 5 | 97 |
| ladle furnace slag | 0-1 | reconst. fishfarm WW | lab – CW | -44.86 | -45.28 | 6 | 9 |
| Sas mixed with limestone | 5-15 | reconst. fishfarm WW | lab – CW | -46.04 | -46.01 | 6 | 12 |
| Sas mixed with limestone | 20-40 | reconst. fishfarm WW | lab – CW | -44.48 | -44.56 | 6 | 8 |
| Sas | 10-30 | reconst. domestic WW | lab – CW | -40.85 | -41.01 | 7 | 11 |
| Sas | 30-100 | reconst. domestic WW | lab – CW | -45.16 | -45.26 | 7 | 8* |
| BOF oxide mixture | 0.003-0.1 | Solution | lab – column | -49.51 | -49.47 | 8 | 8* |
| EAF slag | 20-40 | real domestic WW | pilot – CW | -44.07 | - | 9 | * + |
| BOF slag | 20-40 | real domestic WW | pilot – CW | -43.52 | - | 9 | * + |

252 *: all data below pH 10 for these studies. Data was not considered for calculation of global K_{sp}

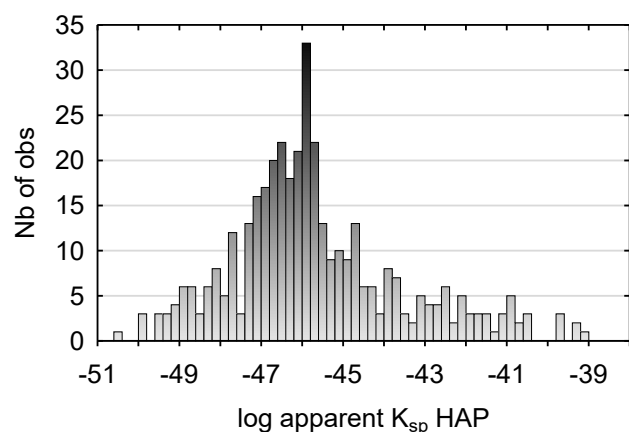
253 +: single K_{sp} calculated from reported mean values for pH, o- PO_4 and Ca

254 Sas: same as present study; WW: wastewater; CW: constructed wetland

255 Ref #1: Claveau-Mallet et al., 2012. Ref #2: Claveau-Mallet et al., 2013. Ref #3: Forget, 2001. Ref #4 :

256 Koiv et al., 2016. Ref #5 : Koiv et al., 2010. Ref #6 : Abderraja Anjab, 2009. Ref #7 : Stangart, 2012. Ref

257 #8: Baker et al., 1998. Ref #9: Barca et al., 2013.



258

259 **Figure 1.** Apparent HAP solubility distribution for all reported studies (pH \geq 10; 389 observations).

260 In heterogeneous precipitation, crystal size is a variable following crystal growth on existing seeds,
 261 assuming that all crystals have the same size. The number of seeds (se_{HAP}) increases as homogeneous
 262 precipitation takes place, assuming an initial number of seeds (se_{HAP_0}) and columnar shape. Equations
 263 for HAP_HE specific surface and solubility product are provided in equations 2 and 3.

$$264 \quad \log(K_{spHAP_HE}) = \log(K_{spHAP_bulk}) + \frac{\frac{2}{3}\gamma S_{HAP}}{2.3RT} \quad [2]$$

$$265 \quad S_{HAP} = \frac{(4L_{HAP}+2)MW_{HAP}}{a_{HAP}\rho_{HAP}} \quad [3]$$

266 2.4.2 Slag dissolution

267 Slag composition was simplified to the chemical formula $CaO-0.3CaCl_2$. Exhaustion equations were
 268 determined experimentally (described later), resulting in decreasing functions for saturation pH (pH_{sat})
 269 and dissolution kinetic constant (k_{diss}). k_{diss} was normalized with slag surface as for precipitation
 270 constants. The proposed approach gives flexibility to the model and every specific slag has its own
 271 exhaustion parameters determined from batch tests by regression.

272 In this model, slag dissolution is assumed to be limited by Fick's law of diffusion (Domenico and
 273 Schwartz, 1998) through a crystal barrier that forms uniformly on the slag surface in a thin layer. The
 274 thickness of the crystal barrier (d_{barr}) increased according to CAL, HAP and MON precipitation,
 275 assuming a constant specific surface (S) for slag (equation 4). It was assumed that the type of
 276 precipitation has an influence on the diffusion coefficient (D_{barr}) and that diffusion is easier in a large
 277 and organized crystals framework, compared to numerous small crystals. Mathematically, D_{barr} was
 278 defined with a step function set initially at a high value, and to a lower value when the seed
 279 concentration was doubled. As either dissolution or diffusion rate is the limiting process (the smallest),
 280 the step function was added to consider the passage from dissolution-limiting to diffusion-limiting.

$$281 \quad d_{barr} = \frac{(m_{CAL}+m_{HAP}+m_{MON})\times n}{\rho_{barr}S\times 0.001(1-n)} \quad [4]$$

282 2.4.3 Hydraulic model

283 In continuous flow column simulations, the Advection-Reaction-Dispersion (ARD) equation for 1D flow
284 was used (equation 5). A first-order exchange approximation was added to account for diffusion
285 between effective and immobile porosity (equation 6). The hydraulic model is available in the PHREEQC
286 software (Parkhurst and Appelo, 1999).

$$287 \frac{\partial C}{\partial t} = -v \frac{\partial C}{\partial x} + D^* v \frac{\partial^2 C}{\partial x^2} - \frac{\partial q}{\partial t} \quad [5]$$

$$288 \frac{db_{im}}{dt} = n_{im} \left(1 + \frac{dq}{dC} \right) \frac{dC_{im}}{dt} = D_n (C_e - C_{im}) \quad [6]$$

289 2.5 Numerical simulations

290 Numerical simulations were performed using the PHREEQC software with its IPHREEQC modules for
291 interfacing with MATLAB (Charlton and Parkhurst, 2011).

292 2.5.1 Batch tests

293 The initial solution was simulated with KH_2PO_4 , K_2HPO_4 , CaCl_2 and NaHCO_3 added to pure water. A small
294 amount of HCl or NaOH was included to reproduce the precise pH of the experimental solution.
295 Solutions were equilibrated with HAP and CAL (but no MON) in the EQUILIBRIUM_PHASES block prior to
296 the simulated batch test. Simulated and experimental alkalinity were used for calibration of initial
297 solutions. Slag exhaustion was considered to be constant, therefore, pH_{sat} and k_{diss} were constant
298 instead of being adjusted according to exhaustion equations. pH_{sat} was set as the maximum pH value
299 reached in the experimental batch test. Calcite precipitation was removed from the batch test model, as
300 surprisingly no calcite precipitation occurred in experimental batch tests (no TIC reduction).

301 The model constants were identified by minimizing the misfit between the simulated output and the
302 experimental pH and oPO_4 measurements. The objective function optimization was performed on the
303 log transformed constants k_{diss} , k_{HAP} , k_{MON} , $k_{MONtoHAP}$ and CaO_{in} with the conjugate gradient

304 method and the golden-section search method (Press, 2007). As shown in Table 2, a two-step strategy
 305 was used to achieve satisfactory results and speed-up the calibration process. In the first step, the mean
 306 absolute error between the experimental and simulated pH (F_1) was minimized with large tolerances for
 307 PHREEQC (1E-11) and the optimization algorithm (1E-7 for line search and 0.01 as F stop criteria). Then,
 308 the objective function F_2 was minimized with more demanding tolerances (1E-12 for PHREEQC and line
 309 search, and 0.001 as F stop criteria). Note that CaO_{in} was a little amount of CaO instantaneously
 310 released at the water/slag contact, added for improving the calibration.

311 **Table 2.** Batch test inversion parameters for conjugate gradient method

| Step | Initial values (log) | Objective function |
|------|---|--|
| 1 | -7 for k_{diss} and CaO_{in} -6.5 for k_{MON} -9 for k_{HAP} and $k_{MONtoHAP}$ | $F_1 = \frac{1}{n} \sum_{i=1}^n pH_{i,exp} - pH_{i,sim} $ |
| 2 | Solution from inversion 1 | $F_2 = F_1 + \frac{0.2}{m} \sum_1^m oPO_{4m,exp} - oPO_{4m,sim} $ |

312

313 2.5.2 Exhaustion functions

314 Exhaustion functions were produced by plotting pH_{sat} and k_{diss} against total leached CaO ($CaOl_{TOT}$).
 315 For a given phase i , $CaOl_{TOT}^i$ was calculated by cumulating leached CaO in preceding kinetic tests and
 316 acid bath (equation 7). $CaOl_{BATH}$ was determined by simulating acid bath with PHREEQC, following the
 317 final pH of the acid bath as a target value.

$$318 \quad CaOl_{TOT}^i = 0.5 \times CaO_{KTEST}^i + \sum_{n=1}^{i-1} (CaO_{KTEST}^n + CaO_{BATH}^n) \quad [7]$$

319 Exhaustion functions coefficients were determined by linear regression of pH_{sat} vs $CaOl_{TOT}$ (equation
 320 8) and logistic function regression of k_{diss} vs $CaOl_{TOT}$ (equation 9). Mean regression coefficients were
 321 kept for k_{diss} , but coefficients following the top of the graphical data cloud were kept for pH_{sat} , as

322 pH_{sat} is a saturation state, and we can assume that saturation is controlled by the most reactive
323 particles.

$$324 \quad pH_{sat} = P_2 - \frac{P_2 - P_1}{(1 + e^{-P_3(CaOl_{TOT} - P_4)})} \quad [8]$$

$$325 \quad k_{diss} = B_1 + B_2 CaOl_{TOT} \quad [9]$$

326 In the Gujer matrix, exhaustion functions included additional terms involving porosity and slag density to
327 account for the conversion of $CaOl_{TOT}$ (units of mol/g slag) into X_{CaO} (units of mol/L water) for filter
328 numerical simulations.

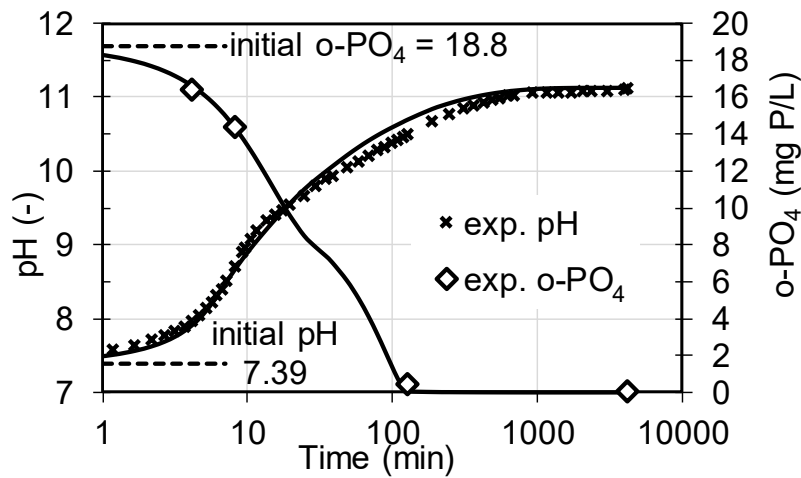
329 2.5.3 Column test

330 The simulated influent was prepared according to the procedure described in the batch tests section.
331 The column test was simulated within KINETIC and TRANSPORT blocks, with 50 numerical cells and a
332 tolerance of 1E-6. Kinetic rates were applied to both mobile and immobile cells. Hydraulic parameters
333 n_e , D^* and D_n were calibrated with each tracer test.

334 3 Results and discussion

335 3.1 Determination of exhaustion equations and precipitation constants

336 In general, batch test calibration was excellent for pH and good for o-PO₄, except for the period 0 to 100
337 min where the model overestimated slightly the o-PO₄ concentration. An example of a well-calibrated
338 batch test (rank 7 out of 84 for global error function) is shown in Figure 2. No TIC reduction was
339 observed. Absence of CAL precipitation in batch tests was not expected, as calcite was precipitated in
340 column tests and is frequently observed in slag filters (Claveau-Mallet et al., 2013; Liira et al., 2009).
341 Mean precipitation constants were $k_{HAP} = 10^{-11.03} \text{ mol HAP/s m}^2 \text{ slag}$, $k_{MON} =$
342 $10^{-8.67} \text{ mol MON/s m}^2 \text{ slag}$ and $k_{MONtoHAP} = 10^{-8.01} \text{ mol HAP}^2/\text{s mol MON}$.



343

344 **Figure 2.** Example of a batch test calibration. Simulated data is shown with lines. Batch test error

345 functions: 0.09 for pH and 0.15 for o-PO₄.

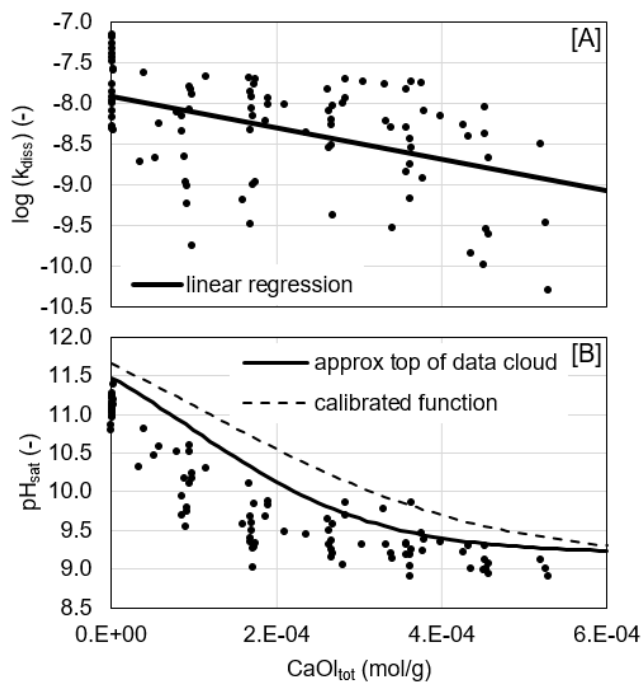
346 pH_{sat} and k_{diss} obtained from all batch tests were plotted against CaO_l_{tot} for the production of exhaustion

347 functions (Figure 3). For k_{diss}, linear regression coefficients were used in column simulations (B₁ = -7.91

348 and B₂ = -1933 g/mol). pH_{sat} exhaustion function had to be slightly increased above the data cloud

349 (discussed later) to improve the calibration (Figure 3B), resulting in coefficients P₁ = 9.1, P₂ = 12.1, P₃ =

350 6000 and P₄ = 1.2E-4.



351

352 **Figure 3.** Exhaustion functions for k_{diss} (A) and pH_{sat} (B). Regression coefficients are provided in text.

353 3.2 Column test calibration

354 An example of tracer test calibration is shown in appendix. Hydraulic parameters D^* (dispersivity) and
355 D_n (exchange factor between mobile and immobile porosity) were roughly constant for 8 tracer tests,
356 while effective porosity (n_e) decreased slightly following the column operation. The n_e decrease was
357 neglected, and hydraulic parameters from tracer test at time 187 were used ($n_e = 0.359$, $D^* = 5$ cm and
358 $D_n = 5 \times 10^{-6} s^{-1}$).

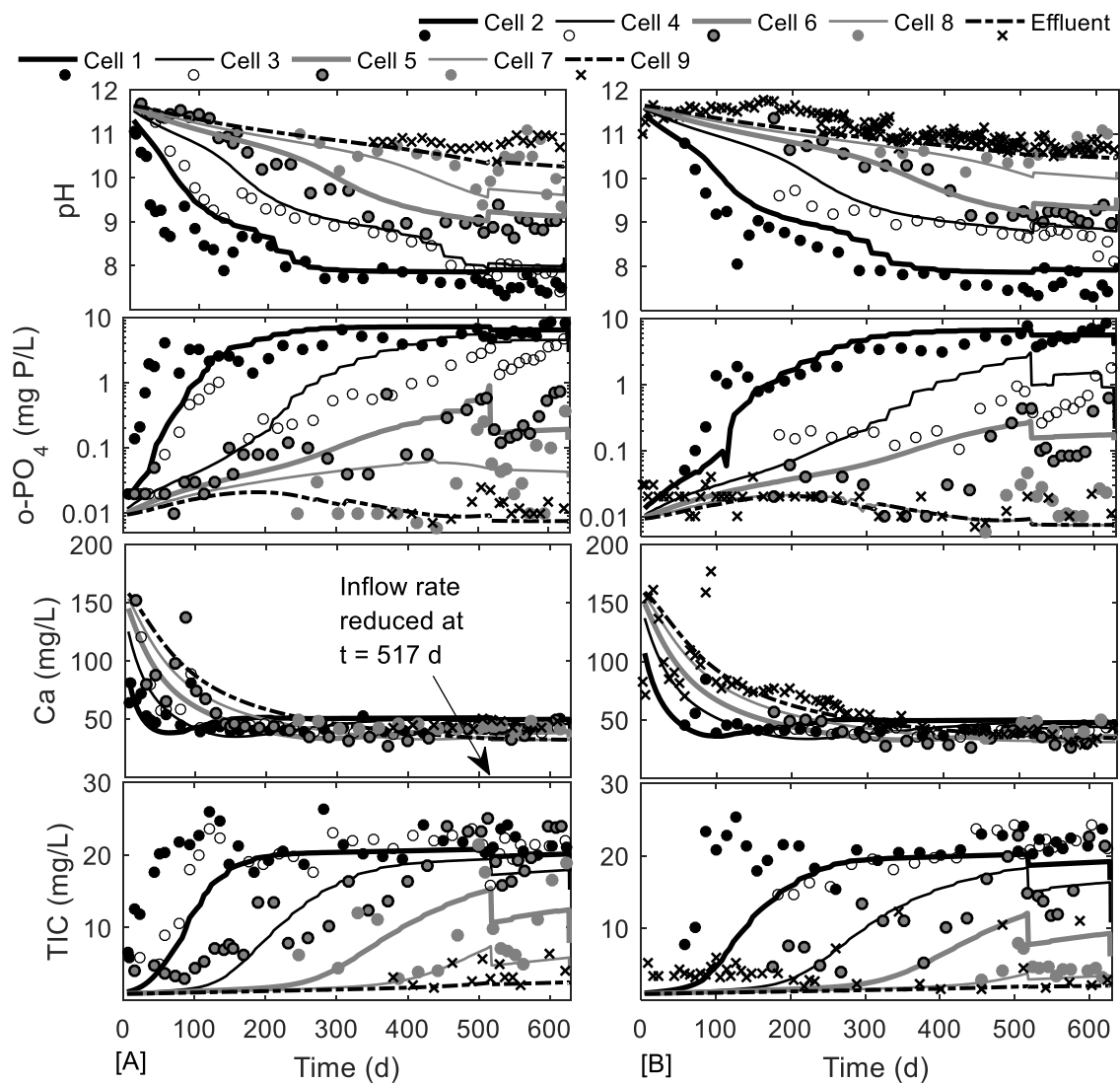
359 Results of numerical simulations are compared to experimental data in Figure 4. pH was correctly
360 predicted for cells 1 to 6 but slightly underestimated for cells 7 to effluent. o-PO₄ was in general
361 successfully predicted, except for cells 1 and 2 in the first 100-200 days, where the o-PO₄ rise was
362 predicted too late. This could be explained by the close position of cells 1 and 2 relative to the influent
363 point resulting in a non plug flow condition for these cells and in some short-circuiting. Calibration of o-
364 PO₄ from cells 5 to 7 was less accurate for the last 100 days, as the model predicted a stable
365 concentration while the experiment showed an increase of almost an order of magnitude. Calcium and
366 TIC calibration were less accurate than those for pH and o-PO₄, but were considered satisfactory. The
367 effect of the influent rate change was correctly predicted by the model.

368 Calibrated constants were $k_{CAL} = 10^{-9} \frac{M}{s m^2}$, $SI_c = 0.2$ and $\rho_{barr} = 2000 \frac{kg}{m^3}$. Precipitation constants
369 for HAP, MON and MONtoHAP were already determined in batch tests and were not changed for
370 column simulations. SI_c was lower than reported values for calcite, which occurs in heterogeneous
371 precipitation over $SI_c = 0.3$ and homogeneous precipitation over $SI_c = 1.5$ (Mayes et al., 2006). ρ_{barr}
372 value was similar to dry density for a natural sand. k_{CAL} was 2.5 orders of magnitude higher than the
373 reported initial value by Mbamba, Tait et al (2015), and monetite constant was in the same order of
374 magnitude as Mbamba's values. In this study, precipitation rates were function of crystal concentration,

375 with initial crystal seeds of $1E-5$ M, while the effect of crystal concentration was not considered in this
376 model.

377 The column was divided in two zones for the calibration of se_{HAP_0} : cells 1 to 6 were set at $2e21$ seeds/L
378 and cells 7 to 9 (and all immobile cells) were set at $5e20$ seeds/L. This refinement was necessary to
379 achieve both $o-PO_4$ calibration of first cells (mainly homogeneous precipitation) and last cells (mainly
380 heterogeneous precipitation). Attributing different se_{HAP_0} values for two zones was considered realistic
381 because it represents a crystal behavior in which at a very low supersaturation index, fewer but bigger
382 crystals are formed. This behavior was confirmed during column dismantling. In cells 8 and 9, a very
383 small amount of precipitates was observed and sampled, with fresh- and unused-looking slag. Several
384 well-formed crystals could be seen by naked eyes only in cells 8 and 9 (3-4 mm in length).

385 The implementation of the diffusion equation is considered a major improvement compared to previous
386 prototype versions of the model. Without the diffusion equation, CaO would always be leached at its
387 maximum capacity (pH_{sat}) and longevity would be highly overestimated. D_{barr} calibration was $1E-10$
388 m^2/s at first and was decreased to $5E-16$ m^2/s when the seed concentration was doubled. Calibrated
389 values of D_{barr} for the two steps are similar to diffusion coefficients observed for clays. A large range was
390 reported for radioactive waste storage applications: from 10^{-17} to $> 10^{-13}$ m^2/s in consolidated clay
391 (Alonso et al., 2009) and 10^{-11} to 10^{-10} m^2/s in altered bentonite (Manjanna et al., 2009).



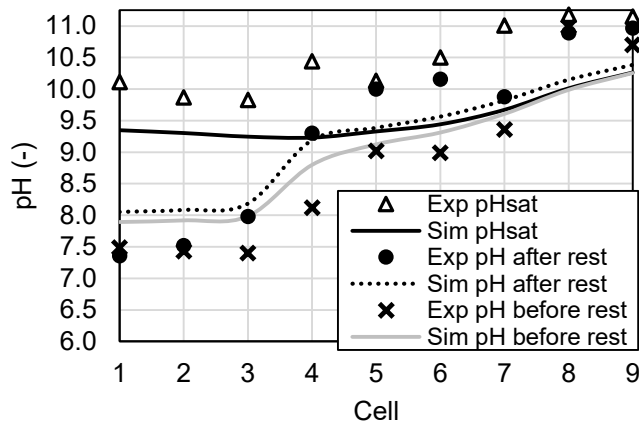
392

393 **Figure 4.** Water composition in a column test for cells 1 to 9 (A) and cells 2 to effluent (B). Experimental
 394 data is shown with dots or x and simulated data with lines.

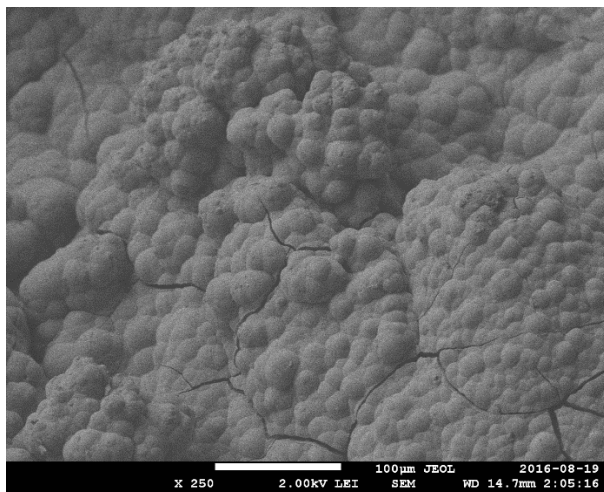
395 3.3 Validation of model hypothesis

396 The diffusion equation can be validated by the robustness of the model regarding pH. The model could
 397 predict pH at the end of operation, pH after the 6-day rest and pH_{sat} (Figure 5). pH was slightly
 398 underestimated for pH_{sat} and pH after rest, but relative trends for pH and pH_{sat} were properly predicted,
 399 as well as the pH increase induced by the 6-day rest. The crystal layer was realistic as uniform crystal

400 deposits were observed by SEM (Figure 6). The presence of cracks induced by air-drying was also
 401 suggesting that a crystal suspension layer was present onto the slag surface. Uniformity of crystal
 402 composition was confirmed by TEM-EDS as CAL and HAP were frequently found in the same crystal at
 403 nanometric scale.



405 **Figure 5.** pH distribution within column at the end of operation (623 days of feeding followed by 6 days
 406 of rest).



407
 408 **Figure 6.** SEM picture of slag grain surface from cell 2 at dismantling.

409 Cristal size in homogeneous precipitation was confirmed by microscope observations. In cells 1 to 3,
 410 where the amount of precipitated HAP was sufficient for measurements, isolated crystals in TEM

411 pictures were measured, resulting in a 35 nm mean value for 505 measurements. A similar value of 24
412 nm was calculated from XRD diffractograms of cells 1 to 3. No specific increase was observed in crystal
413 size from cells 1 to 3, validating the constant crystal size hypothesis for homogeneous precipitation. HAP
414 composition was confirmed by XRD patterns (provided in supporting information). HAP composition for
415 individual crystals from TEM was confirmed by P and Ca presence with EDS. No monetite was detected
416 by XRD and no monetite precipitation occurred in the column simulations while monetite was
417 precipitated in batch test simulations, suggesting that pH rise in column was too fast for monetite
418 formation.

419 The relative small amount of formed HAP in heterogeneous precipitation made impossible XRD or TEM
420 crystal size analysis for heterogeneous HAP. It was possible, however, to analyse the progression of
421 calcite crystal size within the column using XRD. Its size was around 200 nm in cells 1 to 3, increased to
422 900 nm in cell 5, and was over the limit of Scherrer equation in cells 6 and higher. This suggests
423 homogeneous precipitation and constant size in the first cells and heterogeneous precipitation and
424 crystal growth in last cells.

425 Even if a distinction between homogeneous and heterogeneous precipitation was made for calcite, its
426 solubility was kept constant for both conditions. Assuming homogeneous precipitation at 200 nm (as
427 measured in cells 1 to 3) and spherical crystals, the computed solubility product from equation 1 is very
428 close to bulk solubility. While HAP growth decreases its solubility, CAL homogeneous crystals are large
429 enough to neglect this effect.

430 3.4 Model limits and recommendations

431 The main issue regarding the model is the number of batch kinetic tests needed to provide exhaustion
432 equations. The hypothesis of most reactive grains in batch tests conditioning column tests should also
433 be examined, because even if pH_{sat} exhaustion equation was overestimating experimental data, pH in

434 the last cells of columns were underestimated. Work should be done using statistical analysis and theory
435 of artificial granular material sampling (Gy, 1979) for reducing the number of batch tests and
436 transposing correctly batch to column conditions.

437 Calibration of heterogeneous precipitation was limited by experimental data, as last cells did not reach
438 their longevity. Additional studies involving long-term operation of slag filters and breakthrough of last
439 sections of filters, in which heterogeneous precipitation occurred for a while, would be needed for
440 accurate calibration and in-depth study of seeds concentration and type of precipitation. In this paper,
441 two layers of different seeds concentration were proposed, but other formulations would be possible
442 including step functions for seeds VS saturation index, increasing the number of layers or adding a third
443 type of HAP.

444 Further work should be conducted regarding need for refinement of the model. Additional features such
445 as interaction with atmospheric CO₂ or porosity reduction (Courcelles et al., 2011) may be needed in
446 some cases as constructed wetlands. The model could be improved with additional P species (Mbamba,
447 Tait, et al., 2015) or consideration of crystal surface in rate equations. Crystal surface is obviously
448 increasing in this type of process, with long operation time without extraction, but kinetic parameters
449 may be less important than saturation parameters (pH_{sat} and K_{spHAP_HE}). Sensitivity analyses would be
450 needed to assess which aspect should be studied further, slag dissolution kinetics, crystal equilibrium
451 parameters or crystal kinetic parameters.

452 4 Conclusion

453 The first version of the P-Hydroslag model that can be used for prediction of steel slag filter efficiency
454 and longevity was presented in this paper. The objectives were to calibrate the model with experimental
455 data and evaluate the validity and realism of the model. The main outcomes were as follows:

- 456 - A complete model equation matrix was provided. The model included two main kinetic equation
457 sets: a first set for CaO dissolution and a second set for precipitation. CaO dissolution equations
458 included slag exhaustion and CaO diffusion through a uniform crystal barrier on slag particles.
459 Precipitation equations included calcite precipitation, monetite precipitation, transformation of
460 monetite into hydroxyapatite, homogeneous hydroxyapatite precipitation (constant size) and
461 heterogeneous hydroxyapatite precipitation (increasing size). An equation for hydroxyapatite
462 solubility related to crystal size was included. Standard equilibrium reactions were included in
463 the model via the PHREEQC software. The advection-diffusion-reaction model was used as the
464 hydraulic model (1D porous media transport).
- 465 - The crystal barrier hypothesis was confirmed by SEM observations of used slag grains.
466 Homogeneous and heterogeneous precipitation hypothesis was confirmed by TEM crystal size
467 count and XRD measurements.
- 468 - The model and proposed experimental procedure for characterization of slag exhaustion
469 behavior were successful in producing realistic results. Numerical simulations reproduced
470 experimental breakthrough curves (pH, o-PO₄, Ca, TIC) of an upward flow column slag filter.

471 ACKNOWLEDGMENT

472 The authors warmly thank Denis Bouchard, Manon Leduc, Simon Allaire, Simon Amiot and Patricia Bove
473 from Polytechnique Montreal for chemical analyses and technical assistance. They also thank Margit
474 Kõiv-Vainik, from University of Tartu, for providing constructive comments on the manuscript. A special
475 thank is given to Jean-Philippe Massé and Philippe Plamondon, from Polytechnique Montreal CM² lab,
476 for their assistance with TEM, XRD and SEM analysis. Slag material was provided by Philippe Bouchard,
477 from Minéraux Harsco. This project was funded by the Natural Sciences and Engineering Research
478 Council of Canada.

479 REFERENCES

480 Abderraja Anjab, Z. 2009. Development of a steel slag bed for phosphorus removal from
481 fishfarm wastewater (In French). M. Sc. A. thesis, Polytechnique Montreal, Montreal,
482 Canada.

483 Allison, J. D., Brown, D. S., Novo-Gradac, K. J. 1991. *MINTEQA2/PRODEFA2, a geochemical*
484 *assessment model for environmental systems: version 3.0 user's manual*. Environmental
485 research laboratory, USEPA, Athens, Georgia.

486 Alonso, U., Missana, T., Garica-Gutiérrez, M., Patelli, A., Siitari-Kauppi, M., Rigato, V. 2009.
487 Diffusion coefficient measurements in consolidated clay by RBS micro-scale profiling.
488 Applied Clay Science 43, 477-484.

489 American Public Health Association, American Water Works Association, Water Environment
490 Federation. 2005. Standard methods for the examination of water and wastewater 21st
491 ed. Washington, D. C.

492 ASTM. 2004. ASTM C127-04 Standard Test Method for Density, Relative Density (Specific
493 Gravity), and Absorption of Coarse Aggregate. ASTM International: West Conshohocken,
494 PA.

495 ASTM. 2011. ASTM C 702 / C 702 M-11 Standard Practice for Reducing Samples of Aggregate to
496 Testing Size. ASTM International: West Conshohocken, PA.

497 Baker, M. J., Blowes, D. W., Ptacek, C. J. 1998. Laboratory development of permeable reactive
498 mixtures for the removal of phosphorus from onsite wastewater disposal systems.
499 Environmental Science and Technology 32(15), 2308-2316.

500 Barca, C., Troesch, S., Meyer, D., Drissen, P., Andrès, Y., Chazarenc, F. 2013. Steel slag filters to
501 upgrade phosphorus removal in constructed wetlands: two years of field experiments.
502 Environmental Science and Technology 47(1), 549-556. doi:10.1021/es303778t

503 Charlton, S. R., Parkhurst, D. L. 2011. Modules based on the geochemical model PHREEQC for
504 use in scripting and programming languages. Computers & Geosciences 37(10), 1653-
505 1663.

506 Chazarenc, F., Kacem, M., Gerente, C., Andres, Y. 2008. 'Active' filters: a mini-review on the use
507 of industrial by-products for upgrading phosphorus removal from treatment wetlands.
508 In: Proceedings of the 11th Int. Conf. on Wetland Systems for Water Pollution Control.
509 International Water Association, Indore, India, November 1-7.

510 Claveau-Mallet, D., Courcelles, B., Comeau, Y. 2014. Phosphorus removal by steel slag filters:
511 Modeling dissolution and precipitation kinetics to predict longevity. Environmental
512 Science and Technology 48(13), 7486-7493.

513 Claveau-Mallet, D., Lida, F., Comeau, Y. 2015. Improving phosphorus removal of conventional
514 septic tanks by a recirculating steel slag filter. Water Quality Research Journal of Canada
515 50(3), 211-218.

516 Claveau-Mallet, D., Wallace, S., Comeau, Y. 2012. Model of phosphorus precipitation and crystal
517 formation in electric arc furnace steel slag filters. Environmental Science and Technology
518 46(3), 1465-1470. doi:10.1021/es2024884

519 Claveau-Mallet, D., Wallace, S., Comeau, Y. 2013. Removal of phosphorus, fluoride and metals
520 from a gypsum mining leachate using steel slag filters. Water Research 47(4), 1512-
521 1520.

522 Courcelles, B., Modaresi-Farahmand-Razavi, A., Gouvenot, D., Esnault-Filet, A. 2011. Influence
523 of precipitates on hydraulic performance of permeable reactive barrier filters.
524 International Journal of Geomechanics 11(2), 142-151.

525 Cullity, B. D. 2001. Diffraction III: Real Samples. In: *Elements of x-ray diffraction* 3rd ed. Upper
526 Saddle River, NJ: Prentice Hall.

527 Domenico, P. A., Schwartz, F. W. 1998. *Physical and Chemical Hydrogeology* 2nd ed. New York:
528 John Wiley & sons.

529 Forget, C. 2001. Dissolved phosphorus removal from fish farm effluents by reactive granular
530 media (in French). M. Sc. A. thesis, Polytechnique Montreal, Montreal, Canada.

531 Gy, P. 1979. *Developments in geomathematics. theory and practice 4, Sampling of particulate*
532 *materials*. New York: Elsevier Scientific Publications.

533 Kadlec, R. H., Wallace, S. 2009. *Treatment Wetlands* 2nd ed. Boca Raton, FL: CRC Press.

534 Koiv, M., Liira, M., Mander, U., Motlep, R., Vohla, C., Kirsimae, K. 2010. Phosphorus removal
535 using Ca-rich hydrated oil shale ash as filter material - The effect of different phosphorus
536 loadings and wastewater compositions. *Water Research* 44(18), 5232- 5239.

537 Koiv, M., Mahadeo, K., Brient, S., Claveau-Mallet, D., Comeau, Y. 2016. Treatment of fish farm
538 sludge supernatant by aerated filter beds and steel slag filters - effect of organic loading
539 rate. *Ecological Engineering* 94, 190-199.

540 Liira, M., Koiv, M., Mander, U., Motlep, R., Vohla, C., Kirsimae, K. 2009. Active filtration of
541 phosphorus on Ca-rich hydrated oil shale ash: Does longer retention time improve the
542 process? *Environmental Science and Technology* 43(10), 3809-3814.
543 doi:10.1021/es803642m

544 Lizarralde, I., Fernández-Arévalo, T., Brouckaert, C., Vanrolleghem, P., Ikumi, D. S., Ekama, G. A.,
545 Ayesa, E., Grau, P. 2015. A new methodology for incorporating physico-chemical
546 transformations into multi-phase wastewater treatment process models. *Water*
547 *Research* 74, 239-256.

548 Lowell, S., Shields, J. E., Thomas, M. A., Thommes, M. 2004. *Characterization of Porous Solids*
549 *and Powders: Surface Area, Pore Size and Density*. New York: Springer Ed.

550 Lundager Madsen, H. E. 2008. Influence of foreign metal ions on crystal growth and
551 morphology of brushite (CaHPO₄, 2H₂O) and its transformation to octacalcium
552 phosphate and apatite. *Journal of Crystal Growth* 310(10), 2602-2612.

553 Manjanna, J., Kozaki, T., Sato, S. 2009. Fe(III)-montmorillonite: basic properties and diffusion of
554 tracers relevant to alteration of bentonite in deep geological disposal. *Applied Clay*
555 *Science* 43, 208-217.

556 Mayes, W. M., Younger, P. L., Aumônier, J. 2006. Buffering of Alkaline Steel Slag Leachate across
557 a Natural Wetland. *Environmental Science and Technology* 40, 1237-1243.

558 Mbamba, C. K., Batstone, D. J., Flores-Alsina, X., Tait, S. 2015. A generalised chemical
559 precipitation modelling approach in wastewater treatment applied to calcite. *Water*
560 *Research* 68, 342-353.

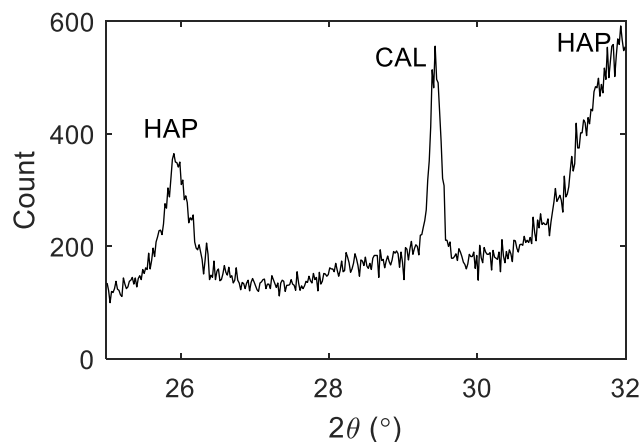
561 Mbamba, C. K., Tait, S., Flores-Alsina, X., Batstone, D. J. 2015. A systematic study of multiple
562 minerals precipitation modelling in wastewater treatment. *Water Research* 85, 359-370.

563 Oelkers, E. H., Bénézech, P., Pokrovski, G. S. 2009. Thermodynamic Databases for Water-Rock
564 Interaction. In: *Thermodynamics and kinetics of water-rock interaction* (Vol. 70, pp. 1-
565 46). Chantilly, VA: Mineralogical Society of America and Geochemical Society.

566 Parkhurst, D. L., Appelo, C. A. J. 1999. *User's guide to PHREEQC (Version 2) - A computer*
567 *program for speciation, batch-reaction, one-dimensional transport, and inverse*
568 *geochemical calculations*. (Water-Resources Investigations Report 99-4259). U. S.
569 Geological Survey, Denver.

570 Penn, C., Bowen, J., McGrath, J., Nairn, R., Fox, G., Brown, G., . . . Gill, C. 2016. Evaluation of a
571 universal flow-through model for predicting and designing phosphorus removal
572 structures. *Chemosphere* 151, 345-355.
573 Press, W. H. 2007. *Numerical recipes: the art of scientific computing* 3rd ed. Cambridge:
574 Cambridge University Press.
575 Stangart, A. 2012. Phosphorus removal from septic tank effluents by coarse steel slag. M. Ing.
576 thesis, Polytechnique Montreal, Montreal, Canada.
577 Stumm, W., Morgan, J. J. 1996a. *Aquatic Chemistry: Chemical Equilibria and Rates in Natural*
578 *Waters* 3rd ed. New York: John Wiley & Sons.
579 Stumm, W., Morgan, J. J. 1996b. Kinetics at the Solid-Water Interface: Adsorption, Dissolution
580 of Minerals, Nucleation, and Crystal Growth. In: *Aquatic Chemistry: Chemical Equilibria*
581 *and Rates in Natural Waters* 3rd ed. New York: John Wiley & Sons.
582 Valsami-Jones, E. 2001. Mineralogical controls on phosphorus recovery from wastewaters.
583 *Mineralogical Magazine* 65(5), 611-620. doi:10.1180/002646101317018433
584 Vohla, C., Koiv, M., Bavor, H. J., Chazarenc, F., Mander, U. 2011. Filter materials for phosphorus
585 removal from wastewater in treatment wetlands-A review. *Ecological Engineering* 37(1),
586 70-89.

587 Appendix



588

589 **Figure A1.** XRD pattern of precipitates sampled in cell #2. Main peaks of HAP and CAL diffractograms are
590 indicated in the figure

Table A1. P-Hydrosrag model matrix

| Phase | Stoichiometry - aqueous | | | | | | Stoichiometry – mineral phases | | | | Rate equation | Equilibrium constants |
|---|-------------------------|--------|-----------|-------------|-------------|--------|--------------------------------|-----|-----|------|---|--|
| | H^+ | OH^- | Ca^{2+} | CO_3^{2-} | PO_4^{3-} | Cl^- | HAP | MON | CAL | HAP2 | | |
| Primary homogenous hydroxyapatite (HAP_HO) | | -1 | -5 | | -3 | | +1 | | | | $r_{HAP_HO} = 0.001k_{HAP}S \frac{(1-n)}{n} \times SI_{HAP_HO} \times SF_{HAP_HO}$ $SI_{HAP_HO} = \log \left(\frac{\{Ca^{2+}\}^5 \{PO_4^{3-}\}^3 \{OH^-\}}{K_{spHAP_HO}} \right)$ $SF_{HAP_HO} = \frac{1}{1 + e^{-50(\log(SI_{HAP_HO}) - \log(SI_c))}}$ | $pK_{spHAP_HO} = 46$ |
| Primary heterogeneous hydroxyapatite (HAP_HE) | | -1 | -5 | | -3 | | +1 | | | | $r_{HAP_HE} = 0.001k_{HAP}S \frac{(1-n)}{n} \times SI_{HAP_HE} \times SF_{HAP_HE}$ $SI_{HAP_HE} = \log \left(\frac{\{Ca^{2+}\}^5 \{PO_4^{3-}\}^3 \{OH^-\}}{K_{spHAP_HE}} \right)$ $SF_{HAP_HE} = 1 - \frac{1}{1 + e^{-50(\log(SI_{HAP_HO}) - \log(SI_c))}}$ | $\log(K_{spHAP_HE}) = \log(K_{spHAP_bu}) + \frac{2}{3} \gamma_{HAP} \frac{S_{HAP}}{2.3RT}$ |
| Monetite (MON) | -1 | | -1 | | -1 | | | +1 | | | $r_{MON} = 0.001k_{MON}S \frac{(1-n)}{n} \times \log \left(\frac{\{Ca^{2+}\} \{HPO_4^{2-}\}}{K_{spMON}} \right)$ | $pK_{spMON} = 7$ |
| Calcite (CAL) | | | -1 | -1 | | | | | +1 | | $r_{CAL} = 0.001k_{CAL}S \frac{(1-n)}{n} \times \log \left(\frac{\{Ca^{2+}\} \{CO_3^{2-}\}}{K_{spCAL}} \right)$ | $pK_{spCAL} = 6.8$ |
| Secondary hydroxyapatite* (HAP2) | | -2 | -4 | | -2 | | | | | +1 | $r_{MONtoHAP} = k_{MONtoHAP} \times SI_{HAP_HO} [MON]$ | $pK_{spHAP_HO} = 46$ |

*: transformation of monetite into hydroxyapatite

Table A1 (followed). Complete P-Hydrosrag model matrix

| | | | | | | | | | | | | | |
|---------------------------------------|--|----|------|--|--|------|--|--|--|--|--|---|-----|
| Slag dissolution | | +2 | +1.3 | | | +0.3 | | | | | | $r_{diss} = A \times SF_{diss}$ $A = 0.001 k_{diss} S \frac{(1-n)}{n} \left(\frac{pH_{sat} - pH}{pH_{sat}} \right)$ $SF_{diss} = 1 - \frac{1}{1 + e^{-50(A-B)}}$ | N/A |
| CaO diffusion through crystal barrier | | +2 | +1 | | | | | | | | | $r_{diff} = B \times SF_{diff}$ $B = \frac{0.5 \times D_{barr} \times (10^{pH_{sat}-14} - \{OH^-\}) \times S \times 0.001(1-n)}{d_{barr} \times n}$ $SF_{diff} = \frac{1}{1 + e^{-50(A-B)}}$ $\log(D_{barr}) = -10 - 5.3 \times \frac{1}{1 + e^{-50 \left(\frac{se_{HAP}}{se_{HAP_0}} - 2 \right)}}$ | N/A |

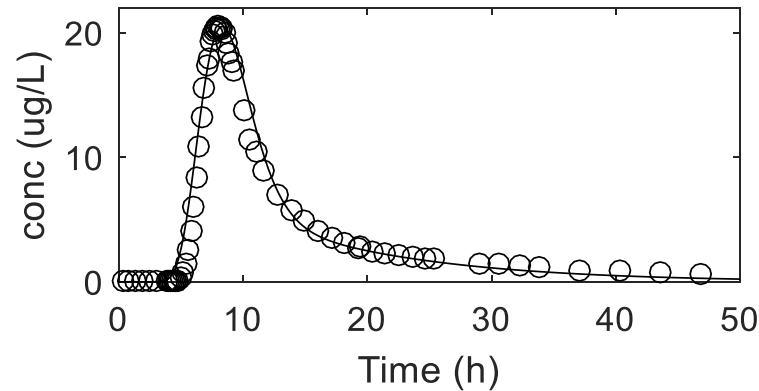


Figure A2. Tracer test experimental data (circles) and numerical calibration (line) (started at Time = 187 d of filter operation)

1 **Detailed equations to complement the model matrix**

2 Advection-reaction-dispersion (ARD) equation for 1D transport and First-order exchange
3 approximation between effective and immobile porosity:

4
$$\frac{\partial C}{\partial t} = -v \frac{\partial C}{\partial x} + D^* v \frac{\partial^2 C}{\partial x^2} - \frac{\partial q}{\partial t} \quad [A1]$$

5
$$\frac{db_{im}}{dt} = n_{im} \left(1 + \frac{dq}{dC} \right) \frac{dC_{im}}{dt} = D_n (C_e - C_{im}) \quad [A2]$$

6 Detailed equations for HAP_HE:

7
$$S_{HAP} = \frac{(4L_{HAP}+2)MW_{HAP}}{\alpha_{HAP}\rho_{HAP}} \quad [A3]$$

8
$$\alpha_{HAP} = \frac{[HAP_HE]MW_{HAP}L_{HAP}^2}{\rho_{HAP}\sqrt[3]{se_{HAP}}} + \sqrt[3]{se_{HAP}^2}\alpha_{HAP_0}^3 \quad [A4]$$

9
$$se_{HAP} = se_{HAP_0} + \frac{[HAP_HO]MW_{HAP}L_{HAP}^2}{\rho_{HAP}\alpha_{HAP_0}^3} \quad [A5]$$

10 Detailed equations for diffusion through crystal barrier:

11
$$d_{barr} = \frac{(100[CAL]+502[HAP]+136[MON]+366[HAP2])\times n}{\rho_{barr}S(n-1)} \quad [A6]$$

12 Detailed equations for exhaustion functions:

13
$$pH_{sat} = P_2 - \frac{P_2 - P_1}{\left(1 + e^{-\frac{P_3}{F}(CaO_{TOT} - F \times P_4)} \right)} \quad [A7]$$

14
$$\log(k_{diss}) = B_1 + \frac{1}{F} B_2 X_{CaO} + \log \left(0.001 S \frac{(1-n)}{n} \right) \quad [A8]$$

15
$$F = \frac{1000\rho_{slag}(1-n)}{n} \quad [A9]$$

16